1. Khalid Subhi Ahmad[1], Mohamad Zoinol Abidin Abd. Aziz[2]

[1]Department of Electronic Engineering, Northern Technical University, (NTU) 41002 Mosul, Iraq
[2]Department of Telecommunication Engineering, Universiti Teknikal Malaysia Melaka, (UTeM) 76100 Melaka, Malaysia
ORCID: 1. 0000-0002-9194-4917

doi:10.15199/48.2021.08.20

Frequency Reconfigurable Microstrip Antenna Array Based on Reconfigurable Defected Ground Structure

Abstract. *In this article, a frequency reconfigurable microstrip antenna array based on a defected ground structure is presented for C-band applications. The proposed antenna used the integration of two patches and the feeding network attached with a circular defected ground structure. The reconfigurable feature of the proposed antenna array is realized using a single switch inserted on the circular defected ground structure to modify the current distribution on the ground plane, which changes the resonance frequency. By switching the switch OFF, the antenna array eligible to resonate at two states and thus array centered at 4.83 and 5.36 GHz simultaneously. While switching ON, the antenna array eligible resonates at three states, and then the antenna array centered at 5, 5.52, and 5.90 GHz simultaneously. Furthermore, design steps, impedance bandwidth, and radiation patterns are introduced for the description and analysis of this antenna array. The finalized antenna array is simulated, manufactured, and measured successfully.*

Streszczenie. W tym artykule przedstawiono układ anten mikropaskowych o rekonfigurowalnej częstotliwości, oparty na strukturze uszkodzonego uziemienia, do zastosowań w paśmie C. Proponowana antena wykorzystywała integrację dwóch łat i sieci zasilającej połączonej z kołową uszkodzoną strukturą uziemienia. Rekonfigurowalna cecha proponowanego szyku antenowego jest realizowana za pomocą pojedynczego przełącznika umieszczonego na kołowej uszkodzonej strukturze uziemienia w celu modyfikacji rozkładu prądu na płaszczyźnie uziemienia, co zmienia częstotliwość rezonansową. Po wyłączeniu przełącznika szyk antenowy kwalifikuje się do rezonansu w dwóch stanach, a zatem szyk jest wyśrodkowany jednocześnie na 4,83 i 5,36 GHz. Podczas włączania, szyk antenowy uprawniony do rezonowania w trzech stanach, a następnie szyk antenowy wyśrodkowany jednocześnie na 5, 5,52 i 5,90 GHz. Ponadto do opisu i analizy tego układu antenowego wprowadzono etapy projektowania, szerokość pasma impedancji i charakterystyki promieniowania. Gotowa szyka antenowa jest z powodzeniem symulowana, produkowana i mierzona. (***Antena mikropaskowa z możliwością rekonfiguracji częstotliwości w oparciu o rekonfigurowalną strukturę uszkodzonego uziemienia***)

Keywords: Antenna array, defected ground structures, frequency reconfigurable antenna, surface current.
Słowa kluczowe: układ anten, kofigurowalna częstotliwość

Introduction

Due to the growing overcrowding of spectrum, frequency reconfigurable elements have achieved considerable estimation, owing to their capability to modify the working frequency band dynamically based on spectrum availability [1]. A microstrip patch element is an essential part of wireless devices, satellite, and microwave communication systems due to its features such as; ease of production, low price, lightweight, and simple structure [2]-[4]. The patch element frequency-reconfigurability can realize by varying the states of radio-frequency switches. Generally, these switches are PIN-diodes, varactor, or microelectromechanical systems (MEMS) [1], [2]. Usually, PIN-diodes are utilized due to their ease of incorporation and decreased cost [5].

Various techniques have been described in the literature to achieve the frequency reconfiguration of an antenna. In [5], the antenna consists of pair sickle-shaped slits on the ground plane (GP) while on the other side of the substrate incorporated the fork-shaped, as feed line. Two PIN diodes are integrated into the slits to achieve two various frequency bands. In [6], the bow-tie patch element is integrated on the two sides of the substrate. PIN-diodes are inserted above the element arms to tune the resonance frequency over the operating band. In [7], a two square ring patch element utilized. By controlling the PIN diode states, the electrical size of the antenna changes and hence achieved reconfigurability. In [8], the integrating fractal slits in the patch antenna produces the meandering of the patch element surface currents, which generates a new resonant frequency. The inserting of PIN diodes within the slit produces a frequency reconfiguration realizable. In [2] placed diodes symmetrically over the right and left side of the patch element. The switch diodes connect between the GP and patch element. The patch operating frequency changed by varying the states of switches. In [9], proposed a hexagonal patch element with H-Tree fractal slits on the GP and the patch element. PIN-diodes are incorporated within the H-slot on the patch to achieve frequency reconfiguring in L and S Bands. In [10], antenna composed of a wideband ellipse patch, coplanar waveguide (CPW) as a feed line, and a couple of squares rings incorporated at the GP to work as a bandpass filter for narrowband operation. A pair of PIN diodes inserted on the slot between the antenna feed line and the square rings to switch between narrowband to wideband operation. In [11], utilized aperture coupled fed patch element. Three slots incorporated at the GP used as a defected ground structure (DGS) for modification in reactance of the antenna. PIN diodes integrated into the antenna to achieve reconfigurability. In [12] proposed a patch element composed of dual elements, the U-shaped element, and the rectangular element. PIN diodes are inserted in the slit between both antennas to produce reconfiguration. In [13] proposed a patch element composed of three sections, ultra-wideband monopole element, with two different types of bandpass filters for the first and the second narrowband mode. The patch element can switch between the two narrowband and the ultra-wideband mode by choosing various RF paths. In [14], the small rectangular and hexagonal slots are integrated into the larger rectangular patch element. The hexagonal slot makes the element operate at dual-band while the small rectangular slit, employed for impedance matching. Pair PIN diodes are integrated over both sides of the hexagonal slot. In [15], the patch element is composed of dual pairs dipoles, the feeding network, switching structure. PIN diodes, inserted between the feeding network and switching structure to achieve reconfiguring. In [16], proposed the planar inverted-F antenna, which consists of, a rectangular patch in the first layer, a substrate in the second layer, an air gap in the third layer, and a GP in the fourth layer. Pair PIN diodes are inserted within the nested slits, etched from the patch element. In [17], the proposed antenna is composed of the

linear monopole, L-monopole, and rectangular patch. Reconfiguration was achieved by inserting a PIN diode and varactor on the slits on the rectangular patch and the L-monopole. In [18], proposed a wideband bow-tie patch element, which is composed of a pair of tapered slot elements, and two kinds of feedings. At the lower part of the radiating antenna, integrated two circular resonators, used as filters. Pin diodes arranged over the slots on the radiating antenna. By switching diodes, the radiator capable switch from a wideband to a narrowband. In [19], the patch element has four slots at the radiator, and two horizontal slots in the GP to improve gain and impedance bandwidth (BW). A PIN diode is inserted at the upper slit, while the second PIN diode is inserted at the lower slit of the radiator. In [20], proposed a C-shaped slot patch element integrated with PIN diodes. In [21], used the edge-truncation of a rectangular element integrated horizontal slot on the GP. Three PIN diodes are inserted over the slit to control the operating frequency. In [22] presented a meandered monopole antenna with a partial GP. The antenna consists of three sections that are linked by two inserted PIN diodes. In [23] used a reconfigurable monopole patch element with a truncated copper GP. Three slots are inserted in the radiating antenna for the incorporating of PIN diodes. In [24], a rectangular patch antenna is integrated with a reversed U rectangular patch. These pair patches are disconnected by a slit. A PIN diode is inserted in the slit to modify the antenna's electrical length and hence change the operating frequency. In [1], the design consists of four slot-fed patch radiators with the DGS in the GP for element size reduction. Reconfigurable feedline used to realize reconfigurability. In [25] used a grid-slotted antenna array. The array consists of 3x3 square patches. The antenna array consists of three metal layers isolated by two substrates. Reconfiguration achieved utilizing two varactors on the grid slot array. In [26], utilized a wideband rectangular dielectric resonator element. The element fed by the microstrip feedline incorporated a reconfigurable bandpass filter to switch between a wideband-to-narrowband by selecting various RF path. In [27], a rectangular patch element is surrounded by four symmetrical parasitic elements. Each parasitic element is linked to the patch element through the varactor diode. By switching varactor diodes, the operating frequency changed. In [28], presented a concentric circle patch element, which is composed of an inner circular antenna and an external ring, separated by a small gap. The branch line coupler is used as a feed network to realize circular polarization. The small slot is selected to integrate the varactor diodes. In [29], proposed Planar Inverted F-Antenna (PIFA) utilizing parasitic tuning elements of different sizes. Parasitic patches are employed to expand the current trajectory on the antenna by enlarging its electrical length. The RF-MEMS switches are used for the sequential connection between the parasitic elements and the antenna. In [30] employed three semicircles DGS integrated with two switches to realize reconfiguring.

Furthermore, few metamaterial methods have been integrated recently to enhance the antenna performance, such as frequency selective surface (FSS) [31],[32], split-ring resonator (SRR) [33],[34], and DGS [35],[36].

In this paper, a frequency reconfigurable microstrip antenna array (MAA) that able to support the C-band application presented. The proposed array is composed of a dual microstrip elements, circular defected ground structure (CDGS), and a single switch that placed within the CDGS slot. By controlling the conditions of the switch, the proposed MAA is capable of produce two working modes. When the switch in the OFF state (Mode-OFF), the MAA resonates at 4.83 GHz and 5.36 GHz simultaneously. While, when the switch is ON (Mode-ON), the MAA resonates at 5 GHz, 5.52 GHz, and 5.90 GHz simultaneously. Inset feed is applied to excite the patch element. This kind of feeding inserts a junction capacitance by inserting a notch. By changing the notch dimension, junction capacitance can be, modified to match the impedance of the transmission feed line to the radiator. This feeding method has cancelled the requirement of an additional matching network for the patch element [12]. The simulation and measurement results of the return loss show good behaviour of the proposed frequency reconfigurable MAA with CDGS.

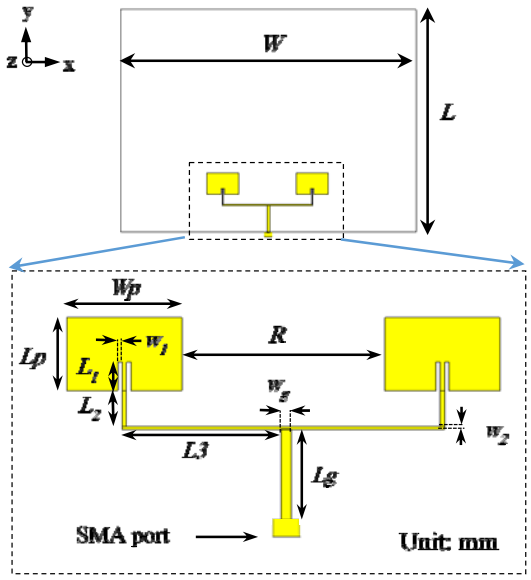

Fig.1. Geometry of the conventional MAA (Unit: mm), front view, where R=31.91, L =134.55, W =165, Wp = 18.09, Lp = 12.9, w1=0.685, w2=0.685, wg=1.583, L1=3.5, L2=6.935, L3=24.55, Lg=16.1

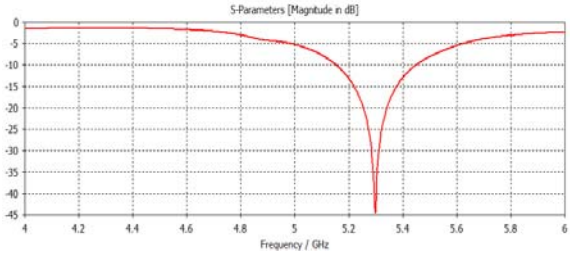

Fig.2. The simulated return loss of the MAA resonant at 4.99 GHz

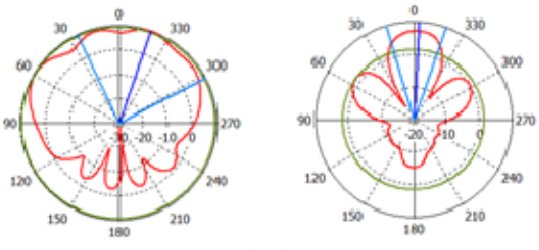

(a) (b)

Fig.3. The simulated far-field pattern of the MAA displayed in Fig. 1
(a) E-plane (b) H-plane
(b)

Reconfigurable MAA design

A. MAA Geometry

This section, in brief, demonstrates the MAA construction. The graphic of the proposed MAA is displayed in Fig. 1. A microstrip transmission line (TL) 1:2 divider is utilized to feed the dual elements, and consequently, the TL

widths are modified based on the power distribution. FR-4 adopted as a substrate (relative permittivity εr = 4.05, loss tangent tan σ = 0.0019, and thickness h =1.6 mm), with a metal thickness of 0.035 mm for both the antenna array and the GP. The MAA design is 165 mm x 134.55 x 1.6 mm, with an inset-feed line. The patch dimension was adopted as Wp = 18.09 mm and Lp = 12.9 mm. The inset feed with a gap $w1$ = 0.685 mm, inset length $L1$ = 3.5 mm. The $L1$ is optimized to make impedance matching amongst the antenna feed line and the radiator. A connector (SMA)-port excitation is used in the simulation. The simulation investigation carried on utilizing Computer Simulation Technology (CST). Fig. 2 shows the simulation result of this MAA and the radiation pattern in Fig. 3.

It is realized the reference MAA resonates at 5.29 GHz with perfect impedance matching. The simulated far-field pattern illustrates a gain of 9.54 dBi in the E-plane and 7.08 dBi in the H-plane. To realize dual-band, CDGS utilized as depicted in the following section.

B. Reconfigurable MAA with CDGS utilizing Single Switch

The defect under the antenna feed line or on the GP disturbs the current distribution of the GP, and it modifies the features of the structure, such as the equivalent inductance and capacitance [37]. To have two various operating frequencies, CDGS integrated on the GP of the MAA depicted in Fig. 4. At first, the conventional MAA constructed to be working at the C band, i.e., 5.29 GHz. Then, CDGS is embedded on the GP of the MAA. Fig. 5 illustrates the MAA achievement with CDGS. It is observed that the operating frequency has been affected by the CDGS, and the MAA together resonates at the 4.83 GHz and 5.36 GHz, i.e., C band.

In this paper, the perfect switch for reconfigurability is a copper bridge. The existence of the copper bridge symbolizes that the switch situation is ON, while the absence of the copper bridge exemplifies that the switch situation is OFF. In this study, the switch element is a typical switch based on the evidence of concept [38],[39]. To realize, frequency reconfigurability a single switch is inserted into CDGS, as depicted as SW in Fig. 6. In this simulation, the typical switch changed with a copper bridge with a dimension of (1mm x 1 mm). The OFF-ON condition of a switch modifies the current distribution. When the switch in the OFF state (Mode-OFF) and thus acts as an open switch, the MAA resonates at 4.83 GHz and 5.36 GHz simultaneously, as illustrated in Fig. 5. Furthermore, when the switch is ON and acts as a closed switch (Mode -ON), the current needs a shorter path, and thus the MAA resonates at 5 GHz, 5.52 GHz, and 5.90 GHz simultaneously, as illustrated in Fig. 7.

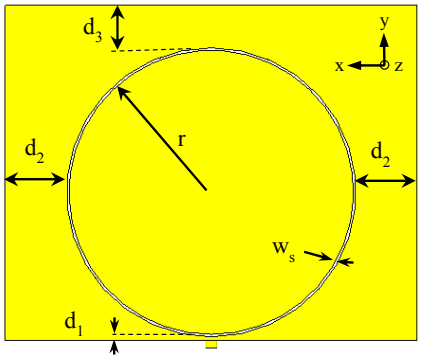

Fig.4. MAA with CDGS back view (Unit: mm), where d1= 0.5, d2= 21.048, d3= 10.05, ws= 1, r= 61

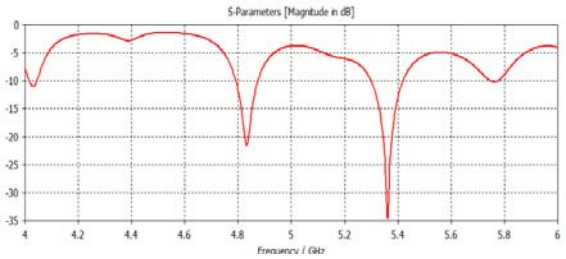

Fig.5. The simulated return loss of the MAA with CDGS resonating at 4.83 GHz and 5.36 GHz, (Mode-OFF)

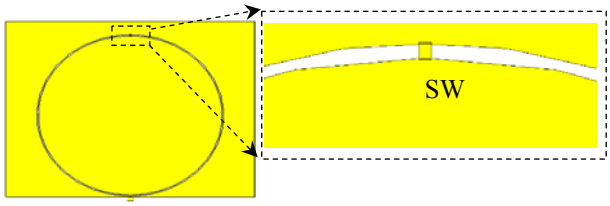

Fig.6. Back view of the MAA embedded CDGS with a copper bridge

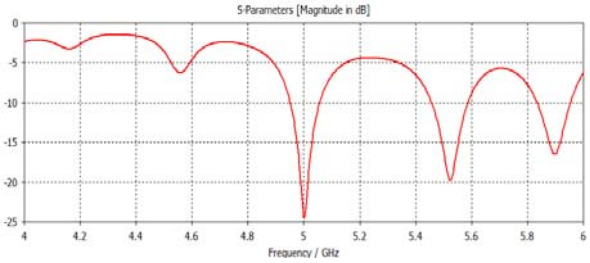

Fig.7. The simulated return loss of the MAA with CDGS resonating at 5 GHz, 5.52 GHz, and 5.90 GHz, (Mode-ON)

Reconfigurable MAA Parametric Study of Radius r

A parametric study is implemented to understand the impact on the performance of the proposed MAA. Using a parametric study of the CDGS radius r can obtain the required operating frequency of the MAA. It is observed varying the parameter r modifies the operating frequency of the MAA. The MAA simulated return loss against the parameter r is illustrated in Fig. 8 and 9 for Mode-OFF and Mode-ON, respectively. As shown in Fig. 8 and Fig. 9, the r is increased from 61 mm to 65 mm, where the chosen r in this work is 61 mm. Table 1 illustrates the two modes of operation (Mode-OFF and Mode-ON) with the achievement of MAA in terms of resonance frequency, BW, and gain for different r. The MAA with r = 61 mm in Mode-OFF operates simultaneously at two resonant frequencies of 4.83 GHz and 5.36 GHz. While Mode-ON operates simultaneously at three resonant frequencies of 5 GHz, 5.52 GHz, and 5.90 GHz, as illustrated in Table 1.

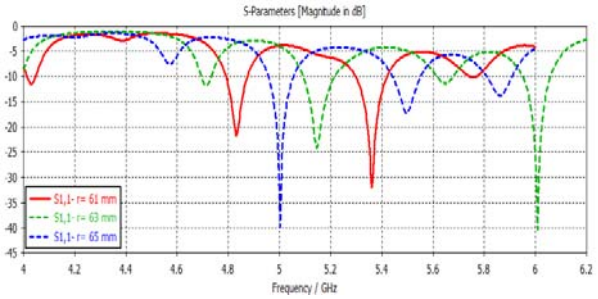

Fig.8. Simulated return losses versus r, where r = 61 mm, 63 mm, and 65 mm, Mode-OFF

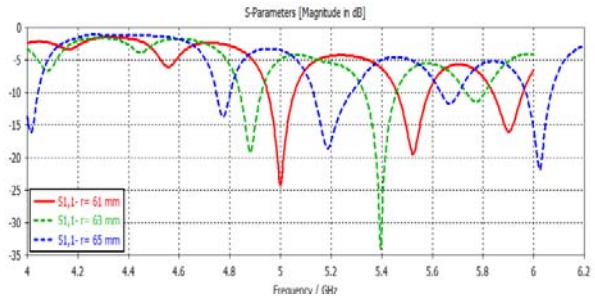

Fig.9. Simulated return losses versus r, where r = 61 mm, 63 mm, and 65 mm, Mode-ON

Table 1. Switch diode state for different r

Mode	Switch State	r value (mm)	operating frequencies (GHz)	BW (MHz)	Gain (dBi)
Mode-OFF Mode-ON	OFF ON	61	4.83, 5.36 5, 5.52, 5.90	80, 110 100, 120, 110	8.57, 8.37 8.39, 7.73, 7.42
Mode-OFF Mode-ON	OFF ON	63	4.70, 5.14, 6 4.88, 5.39	50, 130, 100 80, 130	7.94, 9.34, 3.68 8.03, 7.85
Mode-OFF Mode-ON	OFF ON	65	5, 5.50, 5.87 4.01, 4.77, 5.18, 5.66, 6.02	100, 110, 90 60, 60, 170, 50, 100	8.4, 7.62, 5.36 5.44, 7.14, 9.93, 7.63, 5.37

Experimental results

To prove the proposed design and compare it with measurement results, MAA without CDGS, MAA in Mode-OFF, and MAA in Mode-ON manufactured and measured. For comparison, the single typical switch (SW) is likewise a copper bridge replaced by copper tape in manufacturing. In manufacturing, the copper tape with a 1mm x 1mm size is utilized to approximate the switch SW. The MAA manufactured on the FR-4 substrate with εr = 4.05 and h =1.6 mm. Fig. 10 illustrates the MAA without CDGS, while Fig. 11 displays the front and bottom views, MAA in Mode-OFF. Fig. 12 shows the front and bottom views, respectively, MAA in Mode-ON. The measured return loss S11 compared to the simulated S11. The comparison among measured and simulated return loss results of MAA without CDGS is shown in Fig. 13. The simulated S11 is resonating at 5.29 GHz with a gain of 9.54 dBi, while the measured S11 is resonating at 5.27 GHz. The Agilent N5242A Vector Network Analyzer (VNA) was employed for measurement. Fig. 14 illustrates the comparison among measured and simulated S11 of MAA in Mode-OFF. The simulated S11 resonated simultaneously at 4.83 GHz with 8.57 dBi and 5.36 GHz with a gain of 8.37 dBi, respectively. The measured S11, resonating simultaneously at 4.86 GHz and 5.37 GHz, respectively. Fig. 15 illustrates the comparison among measured and simulated S11 of reconfigurable MAA in Mode-ON, the simulated S11 resonating simultaneously at 5 GHz with a gain of 8.39 dBi, 5.52 GHz with a gain of 7.73 dBi, and 5.90 GHz with a gain of 7.42 dBi, respectively. The measured S11, resonating simultaneously at 5.14 GHz, 5.55 GHz, and 5.83 GHz, respectively. The measured results correspond fine with the simulations.

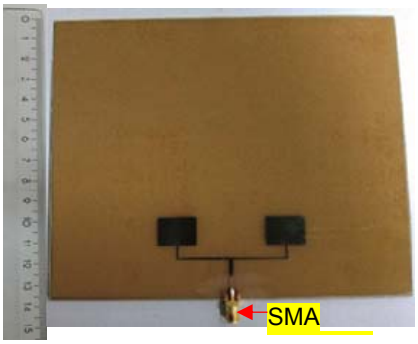

Fig.10. The Manufactured prototype MAA without CDGS, front view

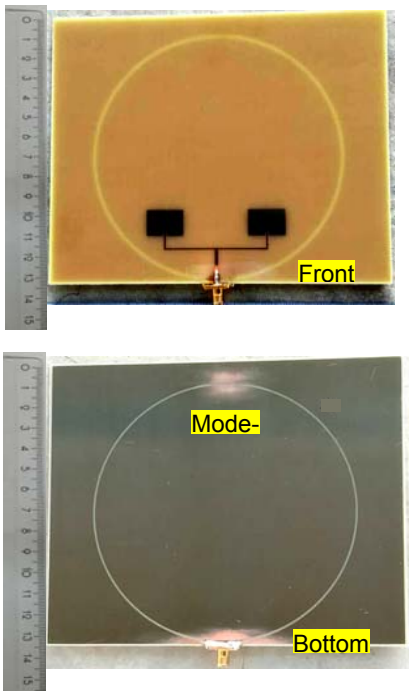

Fig.11. The Manufactured prototype of the proposed MAA with CDGS, Mode-OFF

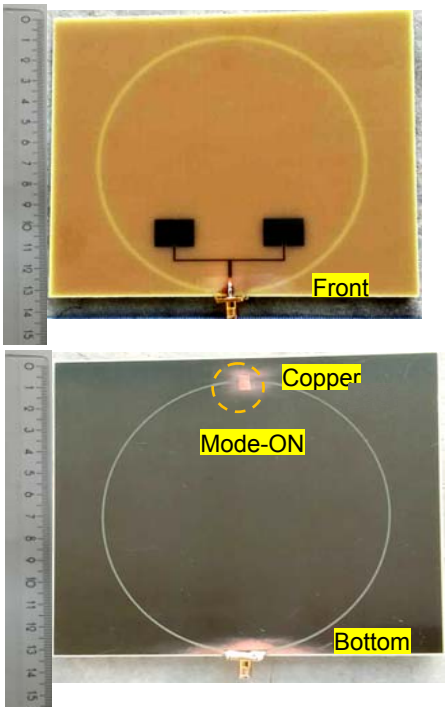

Fig.12. The manufactured prototype of the proposed reconfigurable MAA with CDGS, and a copper tape, Mode-ON

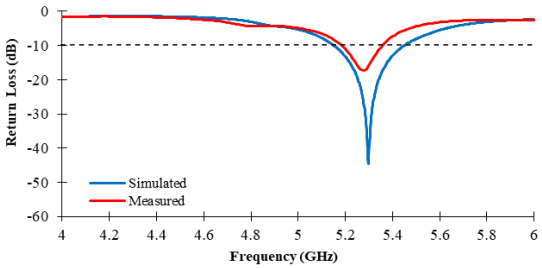

Fig.13. Comparison of measured and simulated S11 of the MAA without CDGS

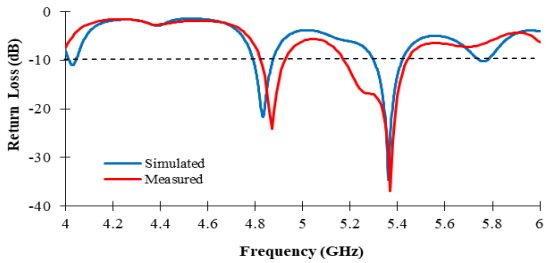

Fig.14. Comparison of measured and simulated S11 of the MAA with CDGS, Mode-OFF

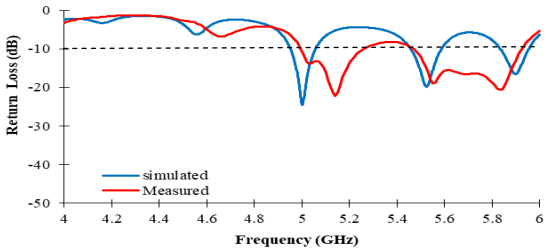

Fig.15. Comparison of measured and simulated S11 of the reconfigurable MAA with CDGS and copper bridge, Mode-ON

Table 2. Different modes of the proposed MAA with resonance frequencies, and BW

Mode	fr	Resonance fr (GHz)		BW (MHz)	
		S	M	S	M
MAA without CDGS	F0	5.29	5.27	290	170
Mode-OFF	F1	4.83	4.86	80	100
	F2	5.36	5.37	130	260
Mode-ON	F3	5	5.14	100	260
	F4	5.52	5.55	120	450
	F5	5.90	5.83	110	450

Frequency (fr), Simulated (S), Measured (M)

The returns loss results S11 in Fig. 13, 14, and 15 are studied, as shown in Table 2. As observed in Table 2, the measured resonance frequencies are higher than the simulated frequencies. This frequency variation may refer to as the soldering influence and fabrication accuracy. Table 2 illustrates two cases for Mode-OFF and Mode-ON with the achievement of MAA in terms of resonance frequency and BW. The maximum difference between the simulated and measured resonance frequencies observed between the simulated frequency 5 GHz and the measured frequency of 5.14 GHz, where it is 140 MHz (2.7 % shift). While the minimum difference between the simulated frequency 5.36 GHz and the measured frequency of 5.37 GHz, where it is 10 MHz (0.18 % shift), as seen from Table 2. With the procedure employed in this proposed work to control the resonance frequencies, the MAA can have five controllable resonance frequencies and four states of return losses. The setup for MAA returns loss and radiation pattern measurements illustrated in Fig. 16 (a) and (b), respectively.

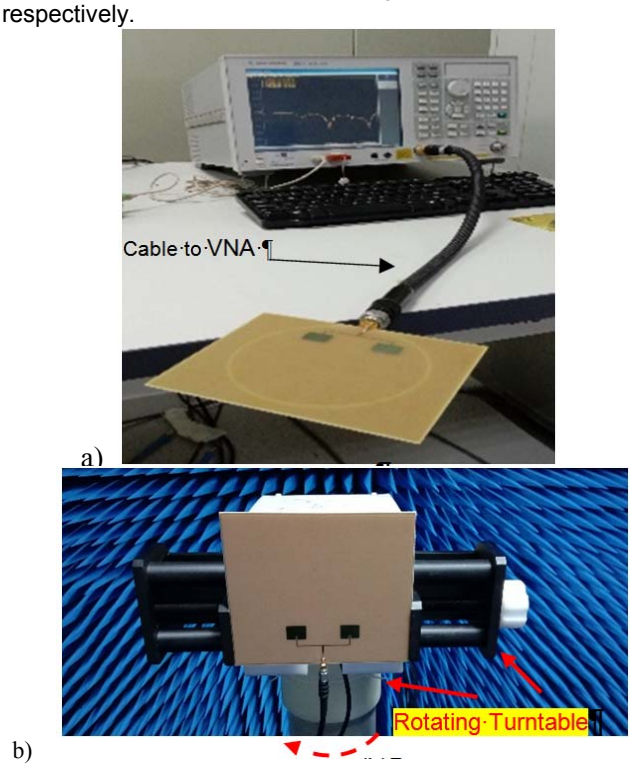

Fig.16. Setup for MAA (a) Return loss measurement, (b) Radiation pattern measurement using an anechoic chamber

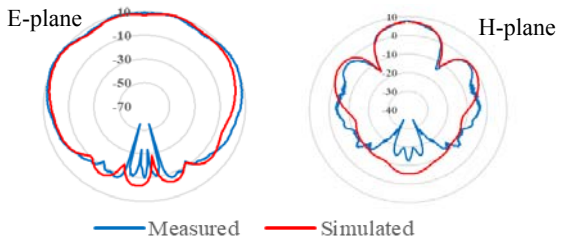

Fig.17. F0, Measured and simulated radiation patterns of MAA without CDGS

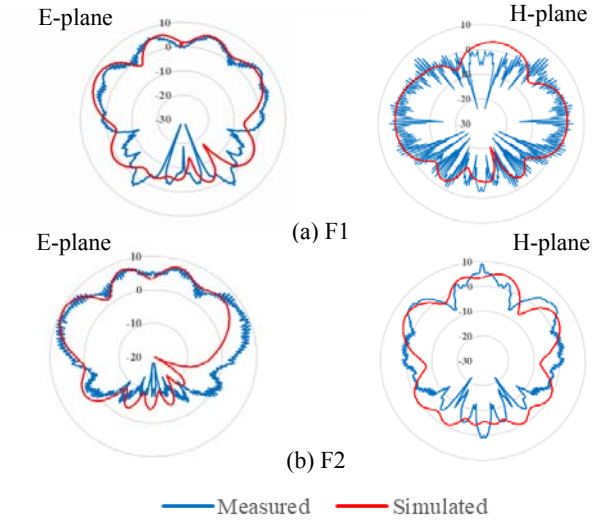

Fig.18. Measur[illegible] E-plane and H-plane of MAA Mode-OFF: (a) F1, (b) F2

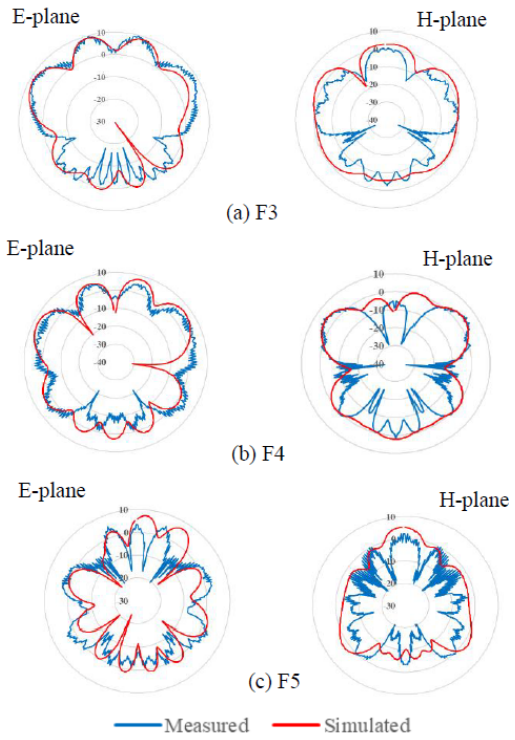

Fig.19. Measured and simulated radiation patterns E-plane and H-plane of MAA Mode-ON: (a) F3, (b) F4, (c) F5

The radiation patterns in the resonance of the MAA without CDGS, reconfigurable MAA in Mode-OFF, and Mode-ON measured in an anechoic test chamber. Fig. 17 to Fig. 19 present the comparison between the measured normalized and the simulated radiation patterns at the resonant frequencies of F0, F1, F2, F3, F4, and F5 in y-z phi=90° (E-plane) and x-z phi=0° (H-plane). Acceptable acquiescence among the simulated and the measured results have been achieved. The proposed MAA shows a nearly omnidirectional radiation pattern for E-plane while the bi-directional for H-plane.

Conclusion

A low-cost reconfigurable MAA printed on FR-4 has been presented. This design employs reconfigurable CDGS in the GP. A single switch integrated within the CDGS to realize frequency reconfigurability. Reconfigurable CDGS change the current distribution on the GP of the MAA, which provides different working bands at; 4.83, 5.36, 5, 5.52, and 5.90 GHz. The return loss S11 of the measurement results employing Agilent vector network analyzer and simulated CST results corresponds with each other with an inconsiderable discrepancy resulting from the fabrication tolerances. The proposed array can be used to support C-band applications.

Acknowledgement

The authors would like to thank the Faculty of Electronics and Computer Engineering and Faculty of Electrical and Electronic Engineering Technology at Universiti Teknikal Malaysia Melaka (UTeM) for the opportunity to use the laboratory equipment for measurement.

Authors: *The first author name is Dr Eng. Khalid Subhi Ahmad, Mosul Technical Institute, Northern Technical University, (NTU) 41002 Mosul, Iraq, E-mail: jarkovo_1988@ntu.edu.com; The second author name is Assoc. Prof. Dr Eng. Mohamad Zoinol Abidin Abd. Aziz, from the Faculty of Electronics and Computer Engineering, Universiti Teknikal Malaysia Melaka (UTeM), Jalan Hang Tuah Jaya, 76100 Durian Tunggal, Melaka. E-mail:mohamadzoinol@utem.edu.my.*

REFERENCES

[1] X. Zhao, S. Riaz, A Dual-Band Frequency Reconfigurable MIMO Patch-Slot Antenna Based on Reconfigurable Microstrip Feedline, *IEEE Access*, vol. 6, pp 41450–41457, 2018.

[2] A. Boukarkar, X. Q. Lin, Y. Jiang, X. F. Yang, A Compact Frequency-Reconfigurable 36-States Patch Antenna for Wireless Applications, *IEEE Antennas Wirel. Propag. Lett.*, vol. 17, no. 7, pp 1349–1353, 2018.

[3] H. H. Keriee, M. K. A. Rahim, N. A. Nayyef, Z. Zakaria, and A. J. A. Al-Gburi, "High gain antenna at 915 MHz for off grid wireless networks," *Bull. Electr. Eng. Informatics*, vol. 9, no. 6, pp. 2449–2454, 2020.

[4] A. J. A. Al-Gburi, I. Ibrahim, and Z. Zakaria, "Gain Enhancement for Whole Ultra-Wideband Frequencies of a Microstrip Patch Antenna," *J. Comput. Theor. Nanosci.*, vol. 17, no. 2–3, pp. 1469–1473, 2020.

[5] M. Y. Zeain et al., "Design of helical antenna for next generation wireless communication," *Prz. Elektrotechniczny*, no. 11, pp. 96–99, 2020.

[6] T. Li, H. Zhai, X. Wang, L. Li, C. Liang, Frequency-Reconfigurable Bow-Tie Antenna for Bluetooth, WiMAX, and WLAN Applications, *IEEE Antennas Wirel. Propag. Lett.*, vol. 14, pp171–174, 2015.

[7] N. Haider, A. G. Yarovoy, A. G. Roederer, L/S-Band Frequency Reconfigurable Multiscale Phased Array Antenna with Wide Angle Scanning, *IEEE Trans. on Antennas and Propag.*, vol. 65, pp 4519–4528, 2017.

[8] O. J. Famoriji, S. Yang, Y. Li, W. Chen, A. Fadamiro, Z. Zhang, F. Lin, Design of A Simple Circularly Polarised Dual-Frequency Reconfigurable Microstrip Patch Antenna Array for Millimetre-Wave Applications, *IET Microwaves, Antennas & Propag.*, vol. 13, no. 10, pp 671–1677, 2019.

[9] A. O. Fadamiro, O. J. Famoriji, R. S. Zakariyya, Z. Zhang, F. Lin, Design of H-Tree Fractal Slots Frequency Reconfigurable Hexagonal Patch Antenna using PIN Diodes, *J. Electromagnetic Waves and Applications*, vol. 33, no. 12, pp 1591–1604, 2019.

[10] M. C. Lim, S. K. A. Rahim, M. R. Hamid, A. A. Eteng, M. F. Jamlos, A. A. Eteng, M. R. Hamid, S. K. A. Rahim, Frequency Reconfigurable Antenna for WLAN Application, *Microw. Optical Technology Lett.*, vol. 59, no. 1, pp 171–176, 2017.

[11] S. Tripathi, N. P. Pathak, M. Parida, A Compact Reconfigurable Aperture Coupled Fed Antenna for Intelligent Transportation System Application, *Int. J. of RF and Microw. Computer-Aided Engineering*, vol. 30, no. 7, pp 1–10, 2020.

[12] I. Nazir, I. E. Rana, N. ul A. Mir, K. Afreen, Design and Analysis of A Frequency Reconfigurable Microstrip Patch Antenna Switching Between Four Frequency Bands, *Progress in Electromagnetics Research C*, vol. 68, pp 179–191, 2016.

[13] M. E. Yassin, H. A. Mohamed, E. A. F. Abdallah, H. S. El-Hennawy, Circularly Polarized Wideband-to-Narrowband Switchable Antenna, *IEEE Access*, vol. 7, pp 36010–36018, 2019.

[14] Tanweer Ali, Rajashekhar C. Biradar, A Compact Hexagonal Slot Dual Band Frequency Reconfigurable Antenna for WLAN Applications, *Microw. Optical Technology Lett.*, vol. 59, no. 4, pp 958–964, 2017.

[15] G. Jin, C. Deng, Y. Xu, J. Yang, S. Liao, Differential Frequency-Reconfigurable Antenna Based on Dipoles for Sub-6 GHz 5G and WLAN Applications, *IEEE Antennas Wirel. Propag. Lett.*, vol. 19, no. 3, pp 472–476, 2020.

[16] F. A. Asadallah, J. Costantine, Y. Tawk, A Multiband Compact Reconfigurable PIFA Based on Nested Slots, *IEEE Antennas Wirel. Propag. Lett.*, vol. 17, no. 2, pp 331–334, 2018.

[17] A. Romputtal, C. Phongcharoenpanich, Frequency Reconfigurable Multiband Antenna with Embedded Biasing Network, *IET Microw. Antennas Propag.*, vol. 11, no. 10, pp 1369–1378, 2017.

[18] D. Abijuru, M. R. Hamid, Pattern and Frequency Reconfigurable Antenna for Body Area Network (BAN), *Jurnal Teknologi*, vol. 76, no. 1, pp 245–252, 2015.

[19] Y. I. Abdulraheem, George A. Oguntala, Abdulkareem S. Abdullah, Husham J. Mohammed, Ramzy A. Ali, Raed A. Abd-Alhameed, James M. Noras, Design of Frequency Reconfigurable Multiband Compact Antenna Using Two PIN Diodes for WLAN/WiMAX Applications, *IET Microw., Antennas Propag.*, vol. 11, no. 8, pp 1098–1105, 2017.

[20] S. Pandit, A. Mohan, P. Ray, Compact Frequency-

Reconfigurable MIMO Antenna for Microwave Sensing Applications in WLAN and WiMAX Frequency Bands, *IEEE Sensors Lett.*, vol. 2, no. 2, pp 1–4, 2018.
[21] Shakhirul Mat Salleh, Muzammil Jusoh, Abdul Hafiizh Ismail, Muhammad Ramlee Kamarudin, Philip Nobles, Mohamad Kamal A Rahim, Thennarasan. Sabapathy, Mohamed Nasrun Osman, Mohd Ilman Jais, Ping Jack Soh, Textile Antenna with Simultaneous Frequency and Polarization Reconfiguration for WBAN, *IEEE Access*, vol. 6, pp 7350–7358, 2017.
[22] Y. Tawk, A. El-Amine, S. Saab, J. Costantine, F. Ayoub, C. G. Christodoulou, A Software-Defined Frequency-Reconfigurable Meandered Printed Monopole, *IEEE Antennas Wirel. Propag. Lett.*, vol. 17, no. 2, pp 327–330, 2018.
[23] I. A. Shah , S. Hayat, A. Basir, M. Zada, S. A. A. Shah, S. Ullah, S. Ullah, Design and Analysis of A Hexa-Band Frequency Reconfigurable Antenna for Wireless Communication, *AEU Int. J. of Electronics and Communications*, vol. 98, pp 1–11, 2019.
[24] Anuradha A. Palsokar, S. L. Lahudkar, Frequency and Pattern Reconfigurable Rectangular Patch Antenna Using Single PIN Diode, *AEU Int. J. of Electronics and Communications*, vol. 125, pp 1–7, 2020.
[25] Y. M. Cai, K. Li, Y. Yin, S. Gao, W. Hu, L. Zhao, A Low-Profile Frequency Reconfigurable Grid-Slotted Patch Antenna, *IEEE Access*, vol. 6, pp 36305–36312, 2018.
[26] B. J. Liu, J. H. Qiu, S. C. Lan, G. Q. Li, A Wideband-to-Narrowband Rectangular Dielectric Resonator Antenna Integrated with Tunable Bandpass Filter, *IEEE Access*, vol. 7, pp 61251–61258, 2019.
[27] C. Guo, Lianwen Deng, Jian Dong, Tulin Yi, Congwei Liao, Shengxiang Huang, Heng Luo, Variode Enabled Frequency-Reconfigurable Microstrip Patch Antenna with Operation Band Covering S and C Bands, *Progress In Electromagnetics Research M*, vol. 88, pp 159–167, 2020.
[28] S. K. Muthuvel, Y. K. Choukiker, Frequency Tunable Circularly Polarized Antenna with Branch Line Coupler Feed Network for Wireless Applications, *Int. J. of RF and Microwave Computer-Aided Engineering*, vol. 29, no. 8, pp 1–9, 2019.
[29] G. Chaabane, V. Madrangeas, M. Chatras, E. Arnaud, L. Huitema, P. Blondy, High-linearity 3-Bit Frequency-Tunable Planar Inverted-F Antenna for RF Applications, *IEEE Antennas Wirel. Propag. Lett.*, vol. 16, pp 983–986, 2017.
[30] K. S. Ahmad, M. Z. A. A. Aziz, and N. B. Abdullah, A Dual-Band Frequency Reconfigurable Antenna Array Based on Reconfigurable Defected Ground Structure, *2020 IEEE Int. RF Microw. Conf. (RFM)*, pp. 1–4, 2020.
[31] A. J. A. Al-gburi, I. M. Ibrahim, M. Y. Zeain, and Z. Zakaria, Compact Size and High Gain of CPW-fed UWB Strawberry Artistic shaped Printed Monopole Antennas using FSS Single Layer Reflector, *IEEE Access*, vol. 8, no. 5, pp. 92697–92707, 2020.
[32] A. J. A. AL-Gburi et al., A Compact UWB FSS Single Layer with Stopband Properties for Shielding Applications, *Prz. Elektrotechniczny*, vol. 97, no. 3, pp. 165–168, 2021.
[33] M. Ibrahim, A. J. A. Al-gburi, Z. Zakaria, and H. A. Bakar, Parametric Study of Modified U-shaped Split Ring Resonator Structure Dimension at Ultra-Wide-band Monopole Antenna, *J. Telecommun. Electron. Comput. Eng.*, vol. 10, no.2, pp. 53–57, 2018.
[34] A. J. A. Al-gburi, I. M. Ibrahim, and Z. Zakaria, "Band-notch effect of U-shaped split ring resonator structure at ultra wide-band monopole antenna," *Int. J. Appl. Eng. Res.*, vol. 12, no. 15, pp. 4782–4789, 2017.
[35] K. S. Ahmad, F. C. Seman, S. A. Hamzah, G. C. Hock, and S. M. Shah, Circuit Model for Microstrip Array Antenna with Defected Ground Structures for Mutual Coupling Reduction and Beamforming Applications, *Int. J. Integr. Eng.*, vol. 13, no. 1, pp. 101–119, 2021.
[36] K. S. Ahmad, M. Z. A. A. Aziz, and N. B. Abdullah, Microstrip Antenna Array with Defected Ground Structure and Copper Tracks for Bandwidth Enhancement, *2020 IEEE Int. RF Microw. Conf. (RFM)*, pp. 1–5, 2020.
[37] M. K. Khandelwal, B. K. Kanaujia, and S. Kumar, Defected ground structure: fundamentals, Analysis, and applications in modern wireless trends, *Int. J. Antennas Propag.*, 2017, pp 1–22, 2017.
[38] N. AL-Fadhali, H. Majid, and R. Omar, Multiband Frequency Reconfigurable Substrate Integrated Waveguide Antenna Using Copper Strip for Cognitive Radio Applicable to Internet of Things Application, *Telecommun. Syst.*, vol. 76, no. 3, pp 1-14, 2020.
[39] B. Li, J. Hong, and B. Wang, Switched Band-Notched UWB/Dual-Band WLAN Slot Antenna with Inverted S-Shaped Slots, *IEEE Antennas Wirel. Propag. Lett.*, vol. 11, pp. 572–575, 2012.